Optical properties of melting first-year Arctic sea ice

Article *in* Journal of Geophysical Research: Oceans · October 2015

DOI: 10.1002/2015JC011163

CITATIONS
53

READS
311

5 authors, including:

Bonnie Light
University of Washington Seattle
77 PUBLICATIONS **3,834** CITATIONS
SEE PROFILE

R. Dadic
Victoria University of Wellington
31 PUBLICATIONS **650** CITATIONS
SEE PROFILE

AGU PUBLICATIONS

JGR

Journal of Geophysical Research: Oceans

RESEARCH ARTICLE

10.1002/2015JC011163

Key Points:
- Albedo and light transmission measured for summer ice cover in Chukchi and Beaufort Seas
- Ponded ice transmits roughly 4.4 times more total energy than bare ice
- Surface scattering and drained layers appear essential for preservation of summer ice

Correspondence to:
B. Light,
bonnie@apl.washington.edu

Citation:
Light, B., D. K. Perovich, M. A. Webster, C. Polashenski, and R. Dadic (2015), Optical properties of melting first-year Arctic sea ice, *J. Geophys. Res. Oceans*, *120*, 7657–7675, doi:10.1002/2015JC011163.

Received 22 JUL 2015
Accepted 28 OCT 2015
Accepted article online 31 OCT 2015
Published online 23 NOV 2015

Optical properties of melting first-year Arctic sea ice

Bonnie Light[1], Donald K. Perovich[2], Melinda A. Webster[1,3], Christopher Polashenski[2], and Ruzica Dadic[4,5]

[1]Polar Science Center, Applied Physics Laboratory, University of Washington, Seattle, Washington, USA, [2]U.S. Army, Cold Regions Research and Engineering Laboratory, Hanover, New Hampshire, USA, [3]School of Oceanography, University of Washington, Seattle, Washington, USA, [4]Department of Atmospheric Sciences, University of Washington, Seattle, Washington, USA, [5]Now at Antarctic Research Centre, Victoria University of Wellington, Wellington, New Zealand

Abstract The albedo and transmittance of melting, first-year Arctic sea ice were measured during two cruises of the Impacts of Climate on the Eco-Systems and Chemistry of the Arctic Pacific Environment (ICESCAPE) project during the summers of 2010 and 2011. Spectral measurements were made for both bare and ponded ice types at a total of 19 ice stations in the Chukchi and Beaufort Seas. These data, along with irradiance profiles taken within boreholes, laboratory measurements of the optical properties of core samples, ice physical property observations, and radiative transfer model simulations are employed to describe representative optical properties for melting first-year Arctic sea ice. Ponded ice was found to transmit roughly 4.4 times more total energy into the ocean, relative to nearby bare ice. The ubiquitous surface-scattering layer and drained layer present on bare, melting sea ice are responsible for its relatively high albedo and relatively low transmittance. Light transmittance through ponded ice depends on the physical thickness of the ice and the magnitude of the scattering coefficient in the ice interior. Bare ice reflects nearly three-quarters of the incident sunlight, enhancing its resiliency to absorption by solar insolation. In contrast, ponded ice absorbs or transmits to the ocean more than three-quarters of the incident sunlight. Characterization of the heat balance of a summertime ice cover is largely dictated by its pond coverage, and light transmittance through ponded ice shows strong contrast between first-year and multiyear Arctic ice covers.

1. Introduction

The partitioning of solar insolation by a summer sea ice cover is a well-established central element of the surface heat and mass budgets of the Arctic Ocean [*Manabe and Stouffer*, 1980; *Jin et al.*, 1994; *Ebert et al.*, 1995]. The magnitude and spectral character of the light field backscattered by, absorbed within, and transmitted through the sea ice cover determine melt at the ice surface and within the ice interior [*Untersteiner*, 1961; *Perovich*, 2005; *Hudson et al.*, 2013], accumulated heat in the ocean beneath the ice [*Maykut and McPhee*, 1995; *Jackson et al.*, 2010], and light available for primary production [see *Palmer et al.*, 2013]. This partitioning is quantified by the apparent optical properties (AOPs) of the ice cover, including albedo, transmittance, extinction, and absorption.

Historically, measurements of the AOPs of sea ice have been made during established ice camps [e.g., *Grenfell and Maykut*, 1977; *Perovich et al.*, 2002; *Light et al.*, 2008; *Nicolaus et al.*, 2010], ship-based cruises [*Frey et al.*, 2011; *Nicolaus et al.*, 2012], and at study sites on landfast ice [*Perovich et al.*, 1998; *Grenfell and Perovich*, 2004; *Hamre et al.*, 2004; *Ehn et al.*, 2008; *Perovich and Polashenski*, 2012; *Nicolaus et al.*, 2013]. Such observations have served as the empirical basis for model parameterizations of the partitioning of solar radiation by the Arctic ice cover in climate models [see e.g., *Briegleb and Light*, 2007; *Holland et al.*, 2012]. Yet, with the exception of the measurements on landfast ice, detailed measurements of light transmittance through the ice cover have been largely biased toward multiyear ice. Dramatic loss of multiyear ice from the Arctic basin over the past decade [*Maslanik et al.*, 2007; *Nghiem et al.*, 2007; *Kwok et al.*, 2009; *Comiso*, 2012] means that these existing data may be less relevant to the sea ice of the future. The growing prevalence of first-year sea ice across the Arctic Basin requires an updated understanding of solar radiation partitioning by this younger and thinner seasonal ice cover.

There are reasons to expect the response to shortwave radiative forcing to be different for first-year ice than for multiyear ice. First-year ice is generally thinner [*Kwok et al*., 2009] and typically has larger pond areal fraction [*Fetterer and Untersteiner*, 1998; *Eicken et al*., 2004; *Perovich et al*., 2011; *Perovich and Polashenski*, 2012] than multiyear ice. Thinner ice is likely to transmit more light to the ocean, promoting the accumulation of heat in the ocean mixed layer as well as fueling primary production within and beneath the ice [*Nicolaus et al*., 2012; *Fernández-Méndez et al*., 2015]. The presence of ponds has notable effect on the radiative balance of the ice [*Inoue et al*., 2008]. Even a skim of liquid water puddled on the ice surface ensures that ponded ice backscatters less light to the atmosphere, permitting more light to penetrate below the surface.

This paper reports measurements of the spectral albedo, spectral irradiance extinction, and spectral and PAR transmittance of shortwave radiation for melting first-year Arctic pack ice observed during the two cruises of the NASA sponsored Impacts of Climate on the Eco-Systems and Chemistry of the Arctic Pacific Environment (ICESCAPE) program in June and July of 2010 and 2011 onboard USCGC *Healy*. Optical observations are related to the physical properties that govern them, and inherent optical properties are suggested for the treatment of shortwave radiative transport by the next generation of sea ice models.

2. Background

Historical measurements of light partitioning serve as the foundation for commonly used model parameterizations of the optical properties of sea ice. In particular, groundwork laid by *Untersteiner* [1961] estimated a bulk extinction coefficient for shortwave solar insolation of 1.5 m^{-1}. *Grenfell and Maykut* [1977] reported spectral albedo and light extinction for sea ice under a wide variety of conditions, including snow covered ice, cold bare ice, and first-year and multiyear bare ice. Their approach to formulating a parameterization was based on the representation of sea ice as two optically distinct layers: a surface scattering layer (SSL) plus an interior layer (IL). The SSL accounts for the large light extinction near the ice surface, and was identified by *Light et al*. [2008] as having effective scattering coefficient typically one to two orders of magnitude larger than the IL. *Light et al*. [2008] expanded this two-layer model to include a third layer, known as the drained layer (DL). This layer sits below the SSL and occupies the remainder of the ice above freeboard. The magnitude of its scattering coefficient is intermediate between that of the SSL and the IL. This three-layer model has been employed to describe radiative transfer in sea ice in the Community Climate System Model version 4 [*Briegleb and Light*, 2007; *Holland et al*., 2012].

Descriptions of light partitioning in first year ice have been carried out by various investigators. *Hamre et al*. [2004] quantified light transmittance through a landfast first-year ice pack as it began to melt. A few data taken by *Light et al*. [2008] include first-year ice cases. *Nicolaus et al*. [2012] undertook a broad look at light transmittance through sea ice in the Arctic Basin, finding enhanced transmission by a first-year ice cover relative to a multiyear ice cover. *Frey et al*. [2011] found considerable spatial variability and a complex transmitted light field beneath a first-year ponded ice cover.

3. Methods

The overarching objective of the ICESCAPE project was to describe the biogeochemical environment where recent seasonal ice retreat has transformed historically ice-covered ocean to seasonally ice-free ocean. The science plan for the ice component of the field work of each cruise included ice stations at locations along transects in the Chukchi and Beaufort Seas. Ten ice stations were established in 2010 and nine ice stations were established in 2011. Figure 1 shows a map of the region with the 19 ice stations indicated. In all cases, the ice was first-year, free of snow, melting, and heavily ponded.

The suite of optical measurements carried out at each ice station included a survey of characteristic spectral albedos and two to three targeted study locations where holes were drilled through the ice for the purpose of lowering light detection sensors beneath the ice cover for measurement of light transmittance and profiles of vertically resolved normalized downwelling planar irradiance.

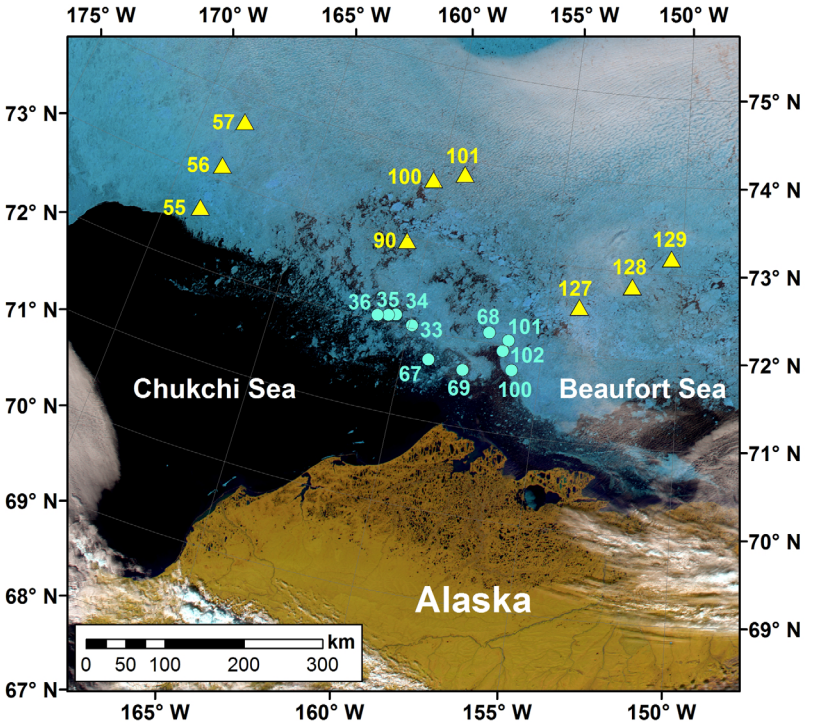

Figure 1. MODIS image from 10 July 2011 annotated with the locations of the ICESCAPE ice stations sampled in 2010 (blue) and 2011 (yellow). Cruise station numbers are indicated for each location.

3.1. Spectral Albedo

The spectral albedo (α_λ) describes the fraction of incident light backscattered by the surface to the atmosphere. For snow and ice, this quantity is generally large at visible wavelengths, and decreases at near-infrared wavelengths, according to the spectral absorption properties of pure ice and liquid brine. Measurements of α_λ are nondestructive and are particularly sensitive to the optical properties of the fragile SSL. Spectral albedo estimates were made using an Analytical Spectral Devices (ASD) FieldSpec Pro spectrophotometer outfitted with a custom built spectralon-wand cosine collector (Figure 2a). Ratios of upwelling irradiance to downwelling irradiance were used to calculate spectral albedo. Relative measurements using a single instrument eliminated the need for absolute radiometric calibration. Albedo measurements were made prior to drilling holes for the under-ice measurements such that the ice surface was as undisturbed as possible.

3.2. Spectral and PAR Transmittance

The transmittance of light through the ice cover was estimated by simultaneously observing downwelling light fields above and beneath the ice. Spectral and PAR sensors were mounted on an articulated arm and lowered through a 10 in. diameter bore hole beneath both bare and ponded ice (Figure 2b). Once the elbow of the arm cleared the base of the ice, the forearm floated until it came to rest against the underside of the ice. The sensors were positioned directly beneath the ice, approximately 1.2 m horizontally from the hole. The arm was equipped with three optical sensors, as pictured in Figure 2c. Downwelling spectral irradiance was measured with an ASD spectrophotometer (prototype instrument built in 1994) coupled to an ASD cosine collector. This instrument is capable of simultaneously measuring light beneath the ice and incident at the surface at wavelengths between 380 and 900 nm. It was necessary to immersion correct the recorded data [*Ehn et al.*, 2008; http://www.biospherical.com/index.php?option=com_content&view=article&id=134:immersion-coefficient&catid=37:calibration&Itemid=137] to account for the discrepancy of sensor-accepted light in air and within water. A sensor-specific correction was estimated separately with the field sensors in a laboratory apparatus. The measured spectral correction varied from a divisor of 0.86 to 0.80 across the visible, decreasing to 0.75 at 800 nm. To correct the submerged sensor, all recorded values were divided by this spectrally dependent correction factor. No attempt was made to correct spectra at wavelengths longer than 800 nm,

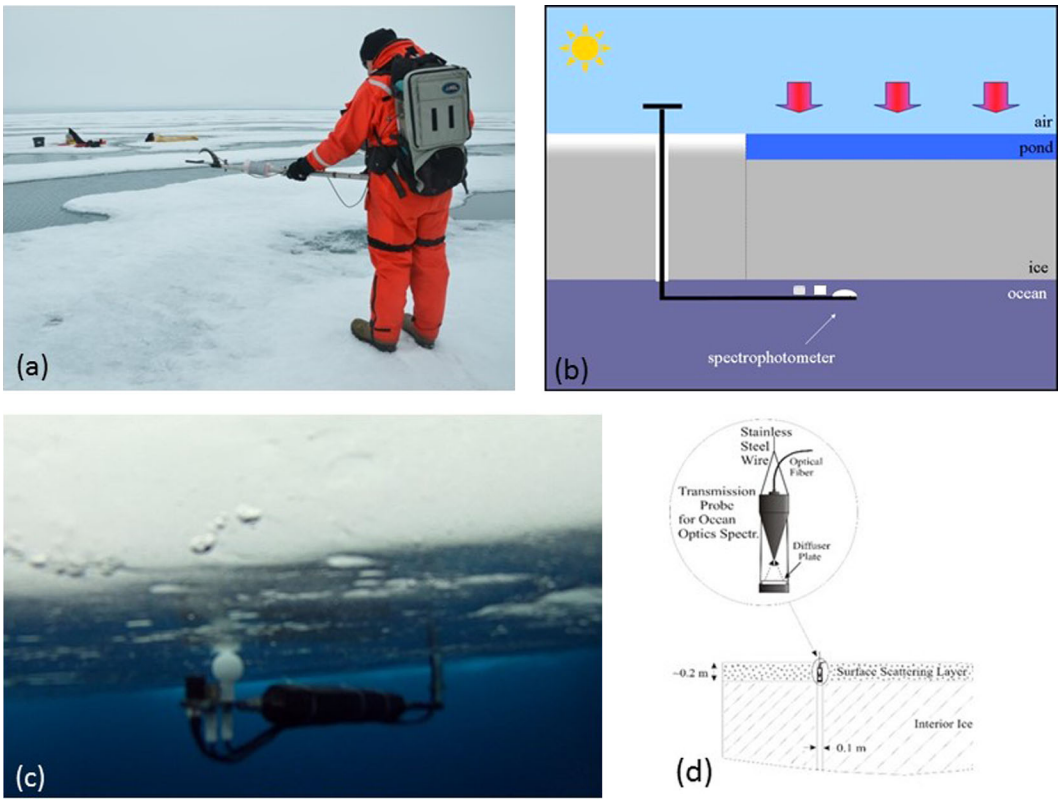

Figure 2. (a) Photograph of the spectral albedo wand being used to measure downwelling flux, (b) schematic of under-ice transmittance measurements, (c) photograph of the under-ice arm, and (d) schematic of the vertical profiler measurements (adapted from *Light et al.* [2008]).

since little light penetrates through the ice at these wavelengths. Downwelling PAR (400–700 nm) planar irradiance was measured independently with a LiCor LI-192 sensor, and downwelling PAR scalar irradiance with a LiCor LI-193. The three sensors were mounted in close proximity on the under-ice arm, but instrument shadowing was estimated to be negligible. Surface reference measurements were made using an additional pair of spectral and PAR sensors. It was not possible to exactly level the beneath-ice sensors, but we estimated they were within 1 or 2 degrees from horizontal while measurements were being recorded.

3.3. Downwelling Normalized Irradiance Profiles

Incident light not backscattered to the atmosphere penetrates the ice, with some portion ultimately entering the ocean beneath. An optical profiler [*Light et al.*, 2008] was used to collect vertically resolved downwelling irradiance within 2 in. diameter bore holes (Figure 2d). Downwelling irradiance was sampled every 0.1 m as the profiler was lowered through the ice. Variations in incident irradiance were monitored with a companion sensor. These profiles are most informative in the ice interior, away from the air/ice and ice/ocean boundaries and large vertical gradients in scattering associated with the SSL and DL. Vertically resolved spectral downwelling irradiances ($F\downarrow[\lambda, z]$) within the interior were used to estimate spectral extinction coefficients ($K[\lambda, z]$) within the ice interior.

3.4. Ice Physical Property Assessment

The physical properties that determine the optical properties of melting sea ice include ice thickness, surface scattering layer thickness, freeboard height, surface melt pond coverage, ice salinity, density, microstructure (size and number distribution of brine and gas inclusions) and the distribution of any absorbing constituents derived from biogenic or terrigenous sources. At each optics site, a core was removed. The core hole was used to measure ice thickness using a thickness gauge (Kovacs Enterprise; https://kovacsice-drillingequipment.com/), freeboard height using a tape measure along the wall of the core hole, and an estimate of the surface scattering layer thickness using a ruler to scrape the loose material from the wall of

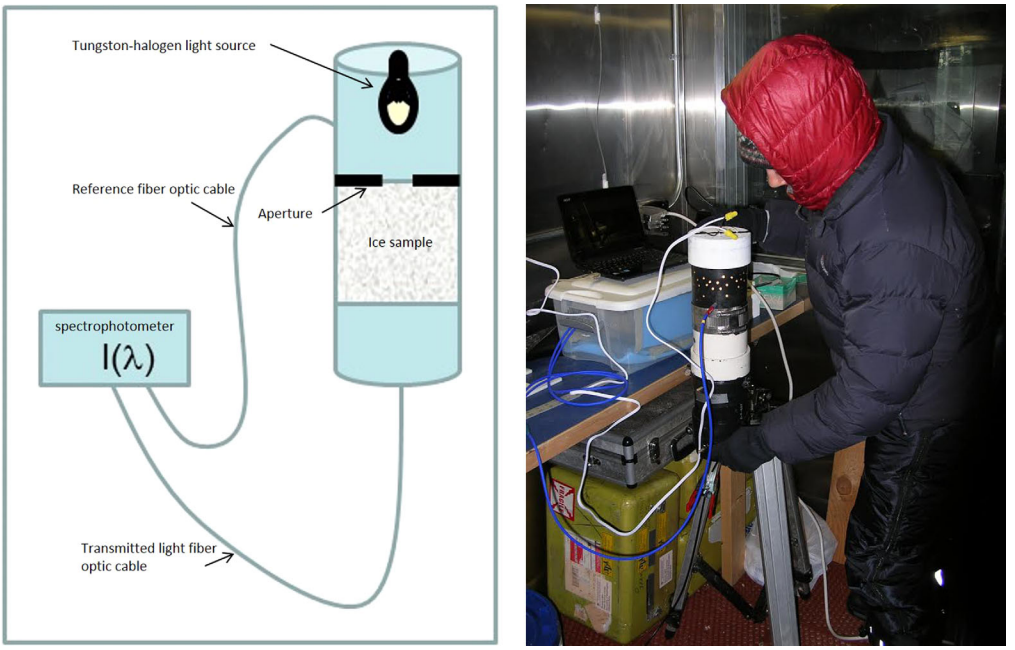

Figure 3. Schematic and photograph of the apparatus used for the laboratory optical measurements in the freezer laboratory.

the hole. Melt pond characteristics (size, depth, spacing) were also recorded. Ice temperature was recorded upon core sampling. Cores were stored frozen on the ship, and subsequently returned to laboratories at UW and CRREL for further analysis. Laboratory measurements made on the cores included vertically resolved profiles of ice density, salinity, and light transmittance experiments. The fragile SSL typically did not survive core sampling intact, so was generally excluded from the samples that were returned to the laboratory. Additionally, ICESCAPE collaborator K. Frey (Clark University) filtered ice samples for typical absorbing constituents found in sea ice, including chromophoric dissolved organic material (CDOM) and chlorophyll.

3.5. Laboratory Light Transmittance

The objective of this work is to not only document the AOPs of the ice cover, but also to gain quantitative understanding of the inherent optical properties (IOPs) of the ice cover and their relationships with the physical properties of the ice. IOPs include scattering and absorption coefficients and information about the single-scattering phase function of the domain. It is difficult to infer IOPs directly from measured AOPs in sea ice because of the large single scattering albedos at visible wavelengths and strong vertical gradients in the scattering within sea ice. *Light et al.* [2008] reported depth-resolved scattering coefficients ranging over three orders of magnitude in bare, melting multiyear ice.

In response to this challenge, a method for assessing vertically resolved scattering in subsections of ice core samples was developed for the laboratory. Figure 3 shows a schematic and photograph of the laboratory apparatus. Samples with height 10 cm were cut from the 10 cm diameter cores and placed inside a cylindrical chamber mounted beneath a tungsten-halogen light source, a translucent optical diffuser plate, and a 30 mm diameter aperture. Diffuse illumination was thus incident only on the center of the core sample. Diffusing the incident light made alignment between the source and the detection optics less sensitive and the aperture served to reduce incident illumination on the sidewalls of the sample. Light passing through the sample was detected with a fiber optic probe coupled to a spectrophotometer (Ocean Optics S2000). An additional channel on the spectrophotometer was used to monitor changes in the bulb output above the ice sample.

Rather than attempting to interpret absolute spectra, transmitted spectra were ratioed to a single reference spectrum. The reference spectrum was recorded at the beginning of each measurement session with pure liquid water in the sample holder. The ratios of spectral light passing through ice samples relative to light

passing through liquid water were compared with radiative transfer model simulations based on calibration data (see below). Since only relative measurements were made, it was not necessary to calibrate the lamp. Core samples were prepared in a freezer laboratory at −15°C and then stored and measured at temperatures as close to their in situ sampling temperature as possible. Typically, the warm, melting ice had lost most, if not all, of its brine, and so its structure was not sensitive to changes in temperature. Considerable care was taken with the colder April sample so that it was not exposed to temperatures high enough to create significant changes in the ice structure.

Calibration of this apparatus was accomplished by measuring light transmission through suspensions of varying concentration of polymer microspheres suspended in water (mean diameter 11 μm; Duke Scientific Corporation catalog 7510A). A two-dimensional Monte Carlo radiative transfer model [*Light et al*., 2003] was used to simulate the radiative transport of light for each concentration of beads in the sample holder, accounting for boundary effects associated with the ceiling, floor, and sidewalls, the finite field of view of the receiving fiber optic probe, and the finite size of the aperture controlling light entering the sample holder. The model treatment assumed the domain was isotropic (the propagation of vertically traveling light is the same as the propagation of horizontally traveling light), even though the two-dimensional boundary conditions and the anisotropy of single scattering events was explicitly treated. Comparison between model simulated transmittances computed over a range of volume scattering coefficients and observed transmittances through the calibration suspensions yielded a calibration relationship. This relationship was then used to infer estimated volume scattering coefficients directly from measured transmittance.

3.6. Radiative Transfer Modeling

A four-stream discrete ordinates radiative transfer model ("4DOM") [*Grenfell*, 1991] was used to simulate the observed AOPs measured in the field. Ice thickness data, measured layer depths, interior ice scattering coefficients inferred from the laboratory optical measurements, and an IOP model were input to 4DOM for simulating the observed spectral albedo and transmittance. Comparisons between modeled and observed AOPs were then used to inform and refine our understanding of vertically resolved IOP models of the ice column.

The process of inferring such an optical model is iterative. Different AOPs are useful for determining the scattering in different layers. Observed spectral albedos reveal information about the IOPs of the surface-most layers of the ice. Scattering coefficients in the SSL are large and independent of wavelength in the visible and near-infrared. At red and near-infrared wavelengths, the penetration depth is relatively small because the single scattering albedo is small due to strong absorption. At shorter wavelengths, the penetration depth is also relatively small, as the single scattering albedo is large within the SSL due to weak absorption and the effects of multiple scattering, thus this light is largely backscattered out of the ice. For these reasons, the spectral albedo of melting sea ice is typically only useful for inferring IOPs at and near the ice surface. The physical and optical properties of progressively deeper parts of the ice column have minimal effect on the albedo.

In contrast, the transmittance responds to the IOPs throughout the entire ice column. However, it is difficult to infer a vertical profile of scattering from the spectral transmittance alone. There may be a number of IOP profiles that satisfy an observed transmittance, even if the spectral albedo is used to infer IOPs near the surface. For this reason, observations made with the spectral profiler, along with the laboratory optical transmittance measurements are helpful for inferring IOPs within the ice interior.

4. Results

4.1. Spectral Albedo

Figure 4 shows spectral albedos measured at all 19 optical study sites. Two distinct classes of ice surface were observed: first-year bare ice and first-year ponded ice. Bare ice is characterized by high albedo at visible wavelengths and moderate albedo at longer wavelengths (pink and red curves). Ponded ice is characterized by a smaller albedo that diminishes quickly at wavelengths longer than 700 nm (cyan and blue curves).

The bare ice albedo observations show modest variability. The optical properties and the physical thickness of the SSL and DL primarily determine the albedo of bare ice, so the moderate variability suggests relatively

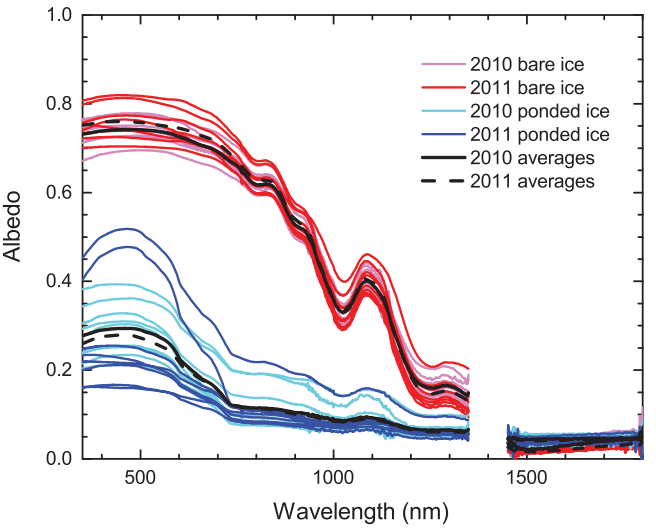

Figure 4. Spectral albedos from all ICESCAPE study sites. 2010 data are shown in magenta (bare ice) and cyan (ponded ice); 2011 data are shown in red (bare ice) and blue (ponded ice). Averages in black for 2010 (solid) and 2011 (dashed). Spectral albedo values near 1380 nm are noisy owing to the small incident radiation at the surface, and thus are not shown.

uniform optical properties in the surface layers of the ice across a broad expanse of ice cover for both summers.

The albedo of ponded ice is smaller than the albedo of adjacent bare ice. The standing liquid water that replaces the highly scattering surface layers of the bare ice significantly reduces backscattering. Ponded ice albedos at visible wavelengths are primarily determined by the optical properties of the ice in the pond floor. The albedo at wavelengths greater than about 750 nm is negligible where the liquid layer is optically thick and little light even reaches the ice. Pond albedos have larger variability than bare ice albedos. This results primarily from the large variety of optical properties found in pond floors and the range of floor thicknesses, and less from the depth of puddled water.

4.2. Spectral and PAR Transmittance

Figure 5a shows observed spectral transmittances and PAR transmittances recorded for the same bare and ponded ice study sites as shown in Figure 4. There are more transmittance measurements than albedo measurements, since some sites had multiple independent transmittance measurements through adjacent bore holes, despite having only a single bare/ponded ice albedo pair. The observed light transmittance depends primarily on whether the surface of the ice is bare or ponded. Bare, melting ice had peak transmittance in the range of 0.05–0.3. Ponded ice had peak transmittance from 0.25 to about 0.73. Peak values typically occurred somewhere between wavelength 470 and 500 nm. As was seen for the spectral albedo, ponded ice spectral transmittance shows more variability than bare ice transmittance. The average ponded ice spectral transmittance was observed to be generally larger in 2011 than 2010, as the bulk of blue curves (2011) are generally larger than the cyan curves (2010). This observation suggests that the 2011 data reflect an ice cover with more advanced melt and more transparent ice beneath the ponds, despite the fact that pond floors were not necessarily thinner in 2011 (average thickness 1.06 m, compared to average of 0.93 m in 2010). The 2011 cruise took place a week later in the summer and the ice concentration was generally lower (blue/white shading in Figure 5c), despite the more northerly station locations.

Figure 5a also shows PAR transmittances (T_{PAR}) as symbols, measured with the LiCor sensors on the same under-ice arm through the same boreholes as the spectral transmittance measurements. T_{PAR} ranged from 0.03 to 0.22 for bare ice and 0.13 to 0.58 for ponded ice. On average, T_{PAR} at a given site matched the spectral transmittance at about wavelength = 590 nm (always between 540 and 660 nm), and are plotted at 585 and 590 nm, even though they represent the full wavelength range of PAR (400–700 nm).

Figure 5b shows $-\ln(T_{PAR})$ plotted as a function of ice thickness. For bare ice cases, "ice thickness" is the thickness of the entire column, from the top of the SSL to the bottom of the IL. For ponded cases, it is the thickness of the ice beneath the pond and excludes the depth of the standing water in the pond. Pond depths ranged from 0.01 to 0.37 m with average depth 0.11 m. If a simple Beer-Lampert Law is applied, and the ice well-described by a representative extinction coefficient, then a linear relationship between ice thickness and $-\ln(T_{PAR})$ would be expected. The magnitude of the slope should approximate a bulk PAR extinction coefficient if the intercept is zero (thickness = 0 m corresponds to transmittance of 1.0). Linear regressions and correlation coefficients are shown with straight black lines for the observed T_{PAR} as a function of ice thickness. The relatively small correlation coefficients and nonzero intercepts indicate that the ice that was measured is not easily described by a simple Beer-Lampert treatment. They do, however, concur

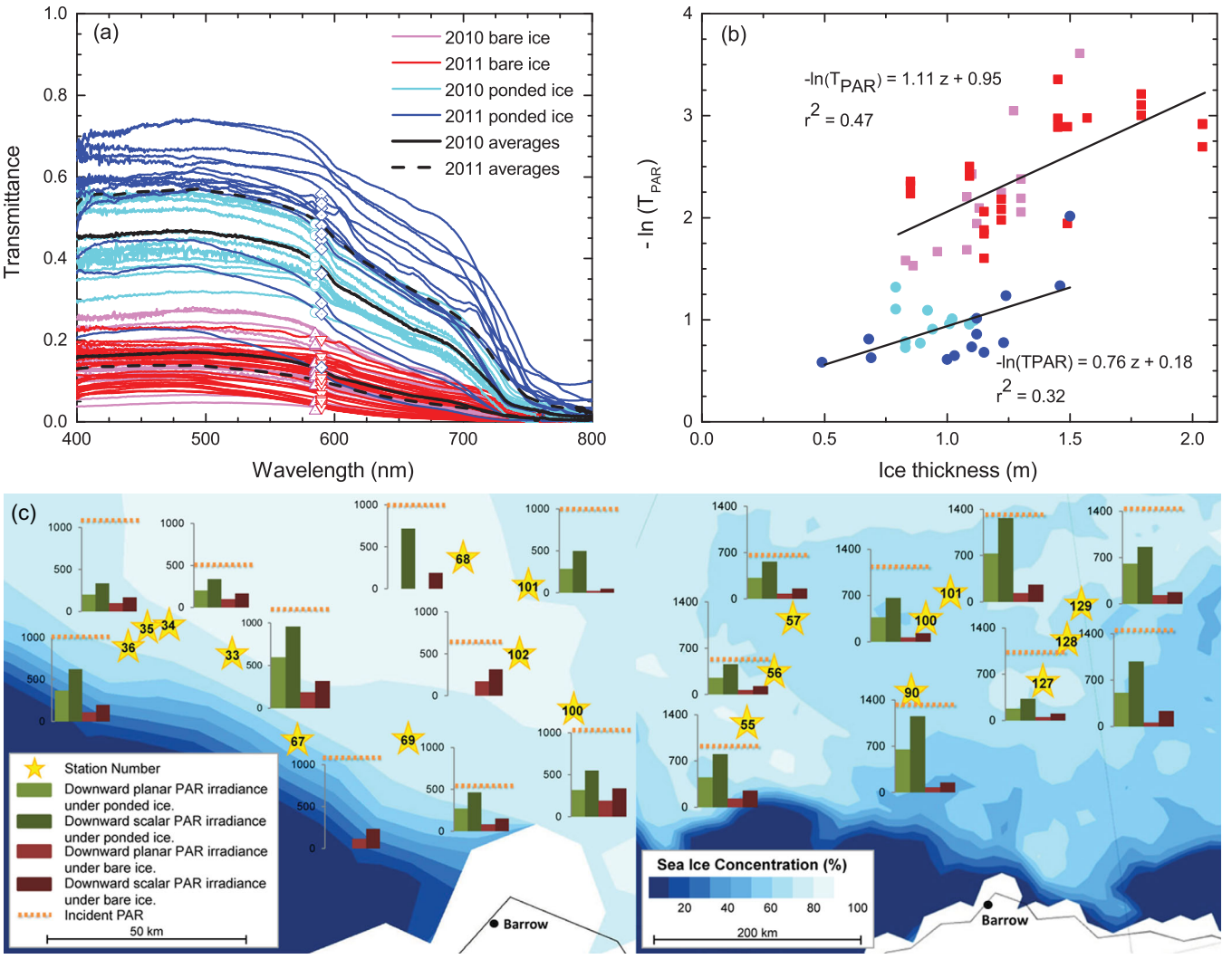

Figure 5. (a) Spectral and PAR transmittances (circles, triangles at 585, 590 nm) for all bare and ponded study sites (b) PAR transmittance as a function of ice thickness, and (c) total transmitted planar and scalar PAR irradiances at all 19 stations measured in 2010 and 2011. Note the larger scale in 2011.

with the idea that extinction is greater in a column of bare ice (larger slope of 1.11 m^{-1}) than it is in ponded ice (slope 0.76 m^{-1}).

Figure 5c shows a map of measured downwelling planar and scalar PAR irradiances beneath the ice for both cruises. Under-ice PAR planar downwelling irradiances reached values as high as 143.2 μmol s^{-1} m^{-2} (bare) and 752.9 μmol s^{-1} m^{-2} (ponded) at Station 6 in 2011. Scalar PAR values on the same date reached 278.1 μmol s^{-1} m^{-2} for bare ice and 1295 μmol s^{-1} m^{-2} for ponded ice. Since these values are not normalized to the incoming irradiance, they fluctuate with solar elevation and the presence of clouds, but these were the largest values measured during these two cruises. There is no attempt to infer either regional or temporal patterns here, rather this map shows the range of PAR values observed above and beneath the ice cover. It is worth noting that skies were generally clearer on ice station days in 2011 than 2010, resulting in larger measured surface incident radiation fluxes, as well as larger measured fluxes beneath the ice cover. However, it is not known whether this contributed to the more advanced state of melt observed in 2011.

4.3. In-Ice Irradiance Profiles

Figure 6a shows vertical profiles of normalized downwelling irradiance at wavelength 500 nm for the six stations where this measurement was made. All profiles were measured within bare ice, except one was measured in ponded ice (blue curve). All show downwelling irradiance decreasing with depth. Spectral irradiance

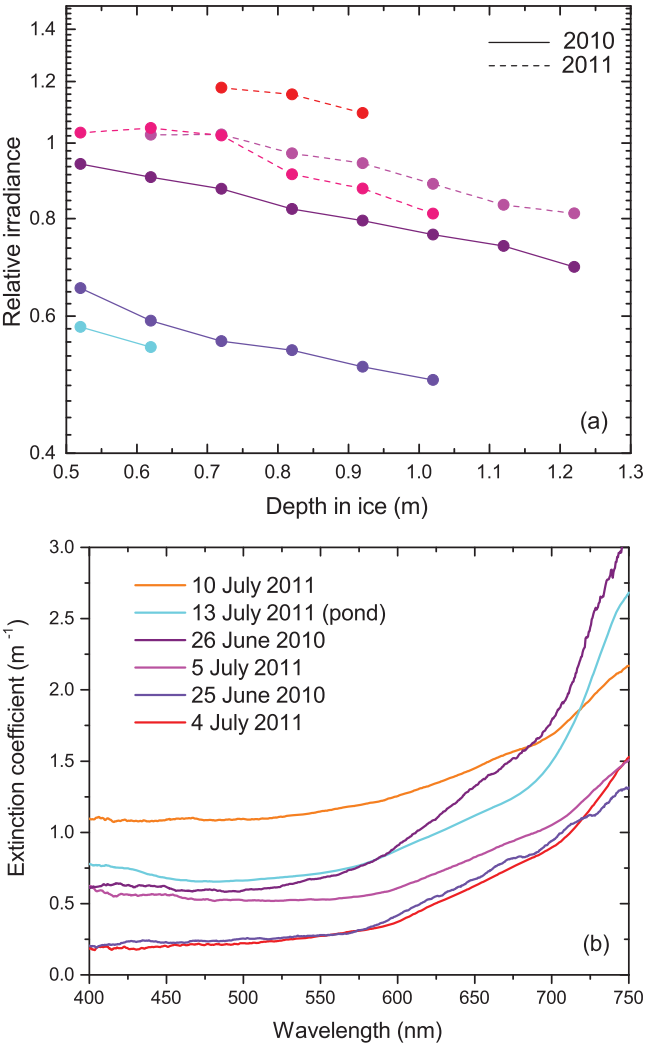

Figure 6. Observations recorded using the vertical profiler showing (a) relative downwelling irradiance at 500 nm as a function of depth, and (b) spectral irradiance extinction coefficients inferred from the irradiance profiles.

extinction coefficients (K_λ) were derived from the irradiance profiles between two depths, z_1 and z_2, using the finite-difference formula:

$$K_\lambda(z) = \frac{-2}{[F_\lambda(z_2)+F_\lambda(z_1)]}\frac{F_\lambda(z_2)-F_\lambda(z_1)}{(z_2-z_1)}$$

where $z = [z_1 + z_2]/2$ and F_λ is the downwelling irradiance at wavelength λ. Figure 6b shows calculated spectral irradiance extinction coefficients for the six measured profiles. The extinction curve for the ponded case is close to the estimated PAR extinction derived from the ponded T_{PAR} measurements shown in Figure 5b (0.76 m^{-1} for the PAR extinction compared with 0.83 m^{-1} for the spectral estimate at 590 nm).

4.4. Ice Physical Properties

The thickness of bare first-year ice measured during ICESCAPE varied between 0.83 and 2.04 m. Freeboard heights ranged from 0.06 to 0.33 m. The lowest ice temperature measured was −1.5°C. The snow had completely melted at all ice stations. The highest bulk ice salinity measured was 3.4 ppt, indicative of the ice having already undergone substantial flushing by surface melt water, but still retaining some salt, discriminating this ice from multiyear ice. Crumbly surface layers had very low density, and because of their fragile nature were not well characterized. Interior ice had measured density values between 625 and 909 kg m^{-3}. Pond depths ranged from 0.01 to 0.37 m. The ice beneath the ponds was generally thinner than neighboring bare ice, and ranged from 0.49 to 1.5 m. Pond horizontal extent varied from less than 1 m to greater than 10 m. We anticipate that the light field within and below the ice reflects the large variability in surface conditions, but in this work, we have only considered case study sites as uniform ice types, and have not considered the three-dimensional effects of this horizontally inhomogeneous ice cover.

Figure 7 shows profiles of ice density and salinity, along with an annotated photograph of a core where the SSL, DL, and IL can be readily identified. The core was photographed in a black tray on the ice immediately after extraction. Density was only measured on the uppermost 0.8 m of the core. Based on these physical properties, we take a three layer IOP model to be appropriate for the radiative transfer modeling in bare ice. For ponded ice, a two-layer IOP model (pond and ice) is justified. The photograph of the core shows the appearance of the interior ice is not uniform, as obvious bands of brighter ice appear below the freeboard level. Also evident are macroscopic brine channels typical of melting sea ice. The laboratory optics were indispensable for determining the vertical variations in scattering through these layers, but these variations appear to be considerably smaller than the variations between the highly scattering SSL, moderately high scattering DL, and the bulk of the IL. There was very little apparent biogenic or terrigenous light absorbing material at most of the study sites, in fact Logvinova et al. (in review) found the ice to have very low CDOM levels. The presence of algae in the ice can also severely affect the transmission of light, but only trace

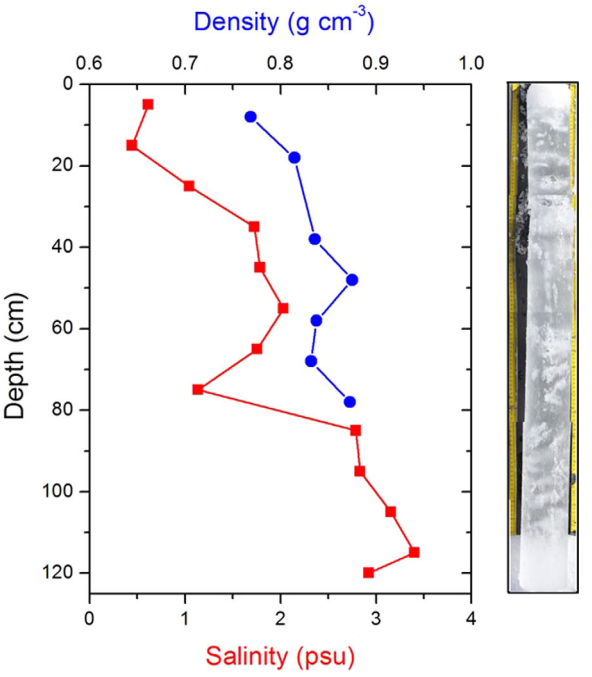

Figure 7. Vertical salinity and density profiles and a photograph of a core extracted from the 19 July 2011 study site. The core photograph is annotated with approximate regions representing the surface scattering (SSL), drained (DL), and interior layers.

amounts of chlorophyll *a* were found in the ice that was sampled. In our modeling, the ice was considered to be free of any absorbing constituents including CDOM, chlorophyll, and sediment.

4.5. Laboratory Optics

Laboratory measurements of the relative light transmittance through 0.1 m thick subsamples of the ice cores provide detailed assessment of the vertical structure of scattering in the ice interior. Figure 8 shows inferred scattering coefficient profiles measured on seven cores from ICESCAPE and one core extracted from cold, level, springtime, first-year fast ice off of Pt Barrow, Alaska in April 2012. The curves show variations in scattering throughout the depth of the ice. The scattering in the uppermost portion of the bare, melting samples should show significantly enhanced scattering, but these surface layers were typically not preserved in the core samples. Since handling these layers is so difficult, our general approach was to use observed spectral albedos to infer optical properties at the ice surface. The cores taken from ponded ice (two blue curves) appeared to have similar scattering as the bare ice sites, but the ponded ice measured on 10 July 2011 had significantly less scattering near the ice surface, just beneath the pond. The gray vertical lines indicate scattering profiles inferred by *Light et al.* [2008] from multiyear ice for bare ice (solid) and ponded ice (dashed). Samples were typically flooded with brine in freezing equilibrium with the sample in the sample holder in an attempt to fill voids in the ice that would have drained when the core was extracted.

The profile for the cold, first-year spring ice (green curve) produced the smallest scattering coefficients measured in the laboratory, consistent with the observation that this ice was highly transparent. Generally, interior scattering coefficients of the cold ice were about 40–50% of the values measured in the interior of the melting ice. This cold ice was snow covered when it was extracted, so it had not yet developed a surface scattering layer. The strong increase in scattering in the uppermost 0.3 m is likely a result of a high salinity surface layer, possibly less ordered crystal structure remaining from the initial ice growth. This uppermost ice sat above freeboard, and may be the precursor to what would ordinarily become a drained layer as melt progresses. The average salinity for the entire core was approximately 4.6 ppt, but because it was still cold, the brine inclusions were small

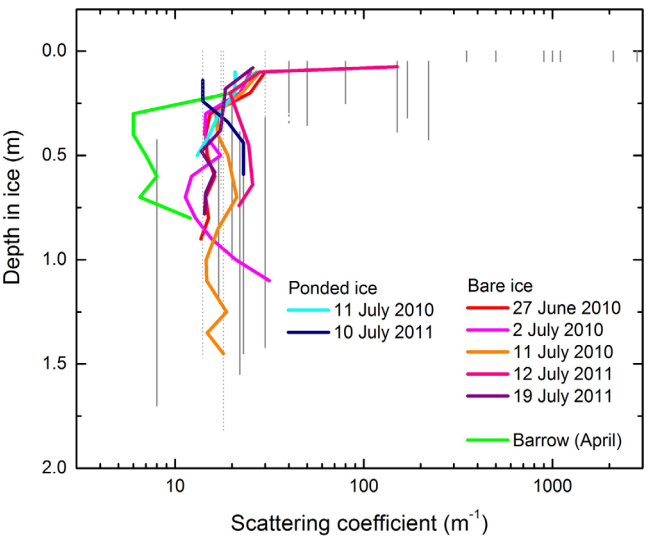

Figure 8. Vertical profiles of scattering coefficient inferred from laboratory transmittance measurements of 10 cm thick core samples. Profiles for multiyear ice, both bare (solid) and ponded (dashed) are shown in gray [see *Light et al.*, 2008].

and isolated. Inferred scattering coefficients for this ice are relatively small, an expected result of small brine inclusions, lack of drainage, and lack of gas bubble formation. This ice was snow covered when sampled, and there is no in situ AOP data for the site where this core was extracted.

The gray lines in the background of Figure 8 indicate inferred scattering coefficients from analysis of field sites measured during the SHEBA experiment. Solid lines were inferred from observations of bare ice; dotted lines from ponded ice. These SHEBA data were taken from different locations at different times throughout the summer, but in all cases the ice was multiyear and melting. The scattering coefficients were inferred using a three-layer radiative transfer model and no attempt was made to resolve vertical variations in scattering within the interior layer. As a result, the interior layer is represented by a constant scattering coefficient. There is ample overlap between the interior measurements made during this study and those inferred from the multiyear ice at SHEBA, suggesting that the interior of melting ice may have optical properties that do not vary substantially between these ice types.

4.6. Radiative Transfer Modeling

Figures 9a and 9b show observed and modeled AOPs for the case study site observed on 19 July 2011. The bare ice at this site was first-year, melting, and undeformed. It was a bit thicker (1.52 m) than the average bare ice (1.30 m) observed during the two field campaigns. The pond was 0.08 m deep (compared to average depth 0.12 m) and the ice beneath the pond was 1.12 m thick (average 1.02 m), but this ice was otherwise deemed representative. The relevant structural features typical of bare, melting sea ice include a porous, crumbly surface scattering layer typically 1–5 cm thick, a drained layer which occupies the remaining portion of the ice above freeboard, and interior ice, which occupies the remainder of the column below freeboard. As outlined by *Light et al*. [2008], the scattering coefficient in the SSL is typically an order of magnitude larger than the DL, which, in turn, is typically an order of magnitude larger than the scattering in the interior. These three distinct layers and the relative effects of their scattering can be seen during visual inspection of an extracted core (as in Figure 7).

Two model simulations are shown in Figures 9a, and 9b; a detailed one uses a seven-layer model for bare ice (three-layer for ponded ice) and a simplified one uses a three-layer model (two-layer for ponded case). Only the simpler IOP model is justified by the overall appearance of the extracted cores, but the more detailed model is useful for explaining spectral variations in AOPs derived from variations in scattering within individual layers. We first describe how the more detailed model was developed and then present the results of the simpler model.

The detailed IOP model was built using five steps: (i) guidance from physical property observations of overall layer structure and appearance, (ii) comparison with spectral albedo for inferring scattering in the surface-most layers, (iii) results from laboratory optical measurements for inferring scattering in the ice interior, (iv) analysis of optical profiler data also for inferring scattering in the ice interior, and (v) comparison with observed spectral transmittance data.

Spectral albedo observations, as shown in Figure 4, were used to infer scattering coefficients in the uppermost surface layer. For bare ice with a developed SSL, the spectral albedo depends most on the optical properties of the surface-most ice. Because absorption by ice depends strongly on wavelength, the wavelengths with the strongest absorption will have albedo sensitive to the shallowest depths and the wavelengths with weakest absorption will have albedo sensitive to properties deeper in the ice. Scattering coefficients are thus assigned to the uppermost layers such that modeled albedos agree with observation, starting with near-infrared wavelengths and working progressively toward shorter wavelengths.

Depending on the magnitude of scattering in the SSL and DL, scattering coefficients in the IL are most readily inferred from the profiler data and the laboratory optics results. The scattering properties of melting ice below the SSL and the DL do not affect the albedo strongly. Total transmittance is useful for overall validation of each optical profile. A seven-layer model produced good agreement with the observations, as shown in Figures 9a and 9b. Table 1 gives the vertical distribution of scattering coefficients used in this highly vertically resolved model.

Development of a three-layer model (two-layer for ponded ice) was desired, since this would provide a framework general enough to accommodate a wide variety of ice conditions. To reduce the seven-layer model to a three-layer model, we combined layers to formulate a simplified model. In particular, the two

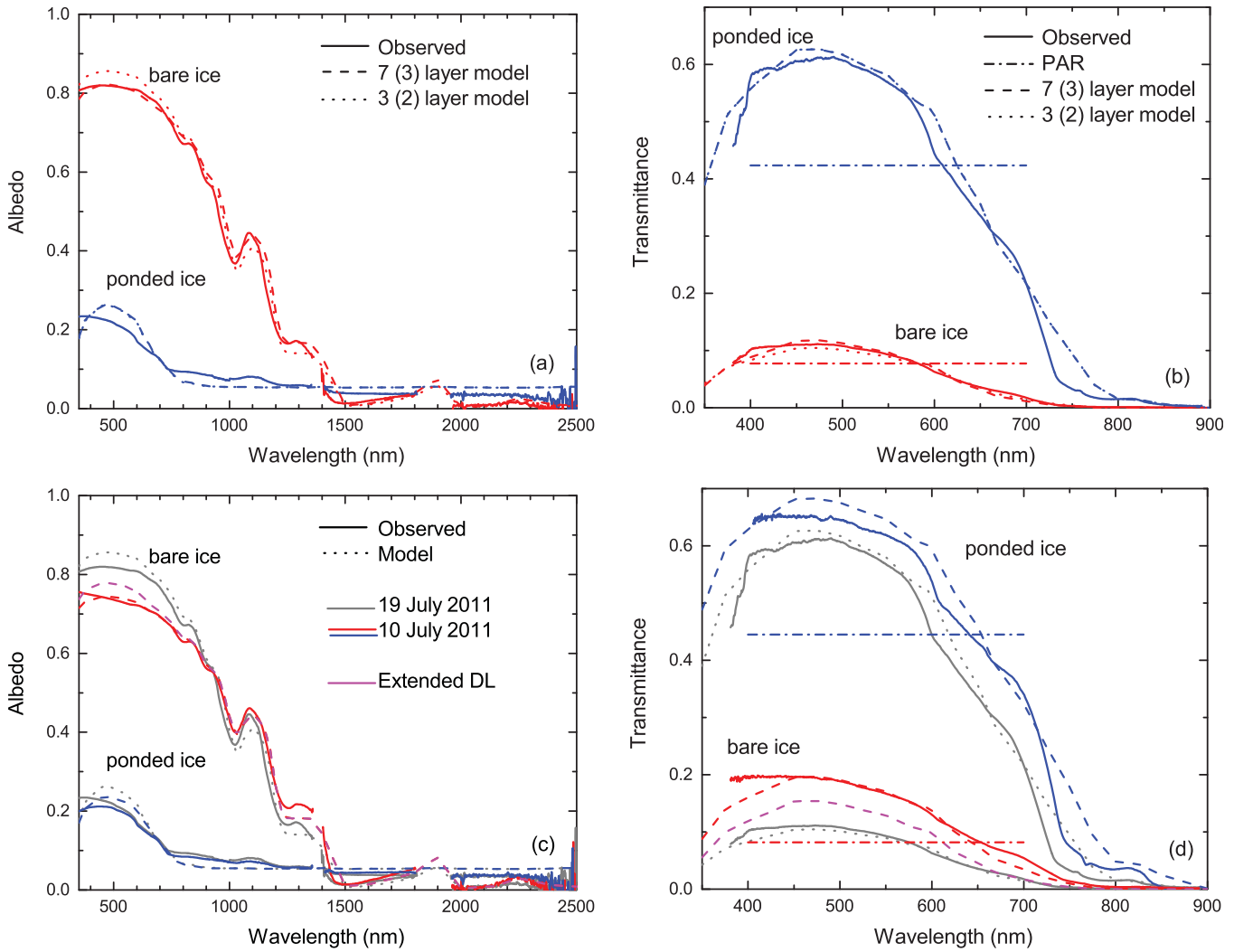

Figure 9. Observed and modeled spectral albedo and transmittance for two case study sites: (a and b) 19 July 2011 and (c and d) 10 July 2011. In all plots, observed spectra are shown with solid lines, observed PAR transmittances with dash-dot lines, and model simulations with dashed or dotted lines. Figures 9a and 9b show model simulations for the enhanced vertical resolution (dashed; seven layers in bare ice, three layers in ponded ice) and a simplified resolution (dotted; three layers in bare ice, two layers in ponded ice). Figures 9c and 9d repeat the 19 July results from Figures 9a and 9b in gray and observed and modeled for 10 July bare ice (red) and ponded ice (blue). Model simulations for bare ice with extended DL are shown in magenta.

uppermost layers were combined to form the SSL, the next three (above freeboard) combined to form the DL, and the two bottommost combined to form the IL. The simplified model is constrained by freeboard depth and total ice thickness. The simplified pond model is restricted to two layers (pond water and interior ice). Calculated optical thicknesses (geometric thickness multiplied by scattering coefficient) were conserved when reducing the detailed model to the simplified model. The resulting scattering coefficients are given in Table 1 and the calculated AOPs are shown in Figures 9a and 9b. The Henyey-Greenstein function with asymmetry parameter 0.94 was used to represent the single scattering phase function for all layers, in both the detailed and the simplified models. This allows comparison of scattering coefficients across layer boundaries, as was done by *Light et al*. [2008].

The 19 July 2011 case was thicker than the average bare ice observed (1.57 m compared to 1.30 m average), and did have significantly more freeboard (0.33 m compared with 0.14 m average). We deemed its optical properties to be representative of the larger area surveyed, yet it clearly had larger than typical freeboard. Given these differences, we also present a comparison between observed and modeled albedo and transmittance for the 10 July 2011 study site. The total bare ice thickness on 10 July was 1.09 m with a freeboard of 0.13 m, which is much closer to the average freeboard observed over the entire experiment. The ponded

Table 1. Idealized Cases of Vertically Resolved Inherent Optical Properties of Observed Bare and Ponded First-Year Melting Arctic Sea Ice as Derived From the 19 July 2011 Case

Geometric Depth (cm)	Refractive Index	Scattering Coefficient (m^{-1})	Modified Geometric Depth (cm)	Refractive Index	Scattering Coefficient (m^{-1})
Seven-Layer Bare Ice			Three-Layer Bare Ice		
1	1.0	2200	SSL—3 cm	1.0	1700
2	1.0	1500	DL—30 cm	1.0	250
10	1.3	450	IL—124 cm	1.3	16
10	1.3	200			
10	1.3	90			
10	1.3	30			
114	1.3	15			
Three-Layer Ponded Ice			Two-Layer Ponded Ice		
10	1.3	0.0001	Pond water	1.3	
10	1.3	18	IL	1.3	13
100	1.3	13			

ice was 0.68 m thick beneath a 0.15 m deep melt pond. Figure 9c shows the observed and modeled spectral albedo and Figure 9d shows observed and modeled spectral transmittance for the 10 July case (red and blue) compared with the 19 July case (gray). As would be expected for the thinner ice, the bare ice albedo is smaller and the bare ice transmittance is larger than the 19 July case. While the pond albedos are similar, the ponded ice transmittance is larger for 10 July compared to 19 July, reflecting the thinner ice beneath the pond. In an effort to account for how much of the bare ice differences can be attributed to difference in DL thickness, the model was used to simulate the 10 July case with increased DL thickness from 0.1 to 0.3 m (shown in magenta in Figures 10c and 10d). The expanded DL accounts for roughly half of the difference in albedo and transmittance at visible wavelengths, suggesting that the DL thickness is a dominant, but not exclusive, factor in determining the AOPs of bare, melting sea ice.

5. Discussion

5.1. Comparing Light Transmittance Through Bare and Ponded Ice

Upon inspection of a field of melting first-year sea ice, the most obvious visual contrast is between bare and ponded ice. These appearances are indicative of the contrasting albedos for these ice types, but they also reveal clues about how the ice physical properties relate to its optical properties, and this may help us to better understand how sea ice responds to the strong shortwave radiative forcing that characterizes the Arctic summer surface heat balance.

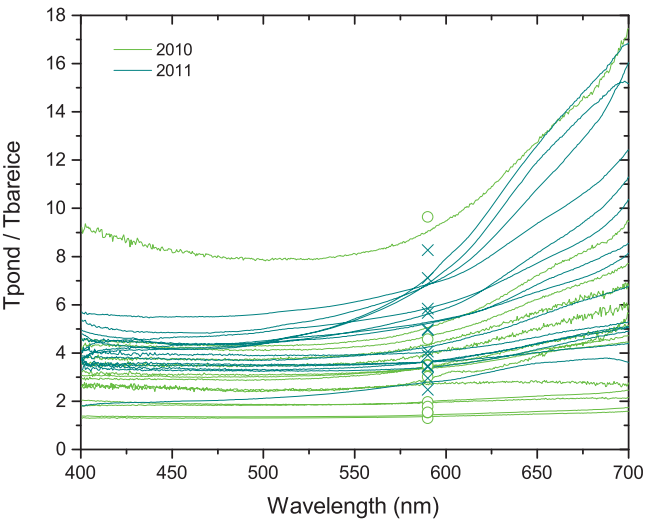

Figure 10. Ratio of ponded ice transmittance to bare ice transmittance for all study sites. 2010 data are indicated by bright green curves; 2011 data by dark green curves. Crosses and circles indicate measured PAR transmittance ratios.

Figure 10 shows the ratio of spectral pond transmittance to spectral bare ice transmittance for all adjacent pond/bare sites measured. The larger the ratio, the larger the light transmittance contrast through adjacent bare and ponded ice areas. Viewed from beneath, sites with large contrast will have the least horizontally homogeneous downwelling light field. Bright green curves show 2010 observations and dark green curves show 2011 observations. Independently measured PAR transmittance ratios are indicated with symbols (o indicates 2010; x indicates 2011). At short wavelengths ($\lambda < 550$ nm), light transmittance through ponded ice is 1.3 to nearly 10 times that through bare ice. This ratio increases with increasing wavelength.

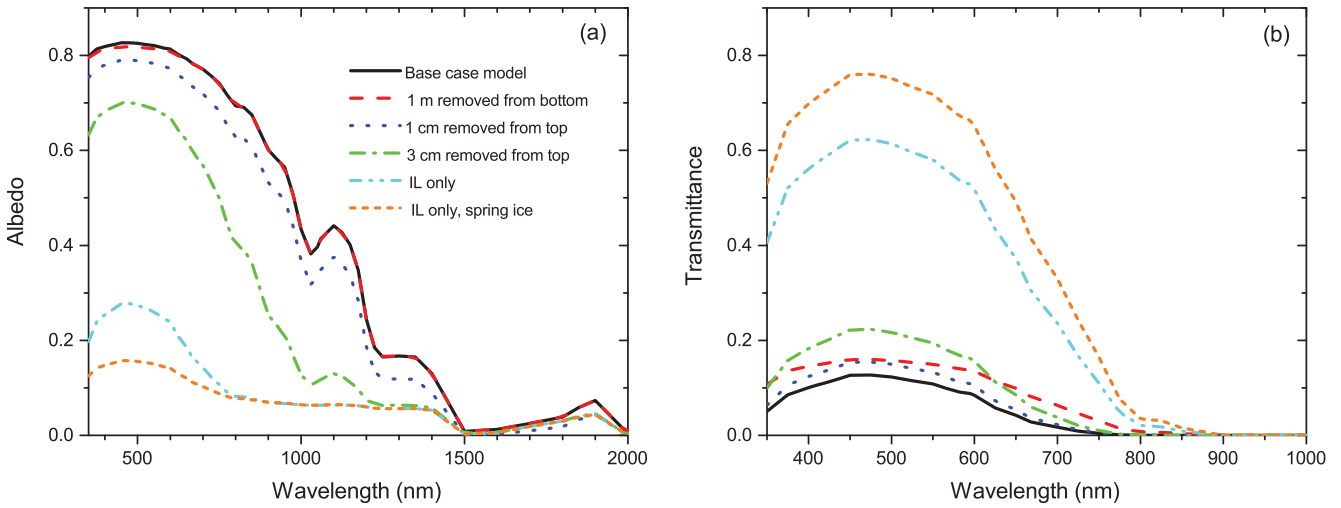

Figure 11. One-dimensional radiative transfer model predicted (a) albedo and (b) transmittance illustrating the effects of the surface scattering layer and drained layer on the apparent optical properties of bare, melting first-year sea ice.

All of the observations of pond/bare ice ratios made during ICESCAPE are clustered around short wavelength ratios less than 6, except for one. The one case with significantly higher ratio was measured on 10 July 2010. The pond transmittance at that location appeared typical, but the bare ice transmittance was the lowest measured during both campaigns. This ice was undeformed, melting, first-year ice. The total ice thickness was 1.54 m, which was thicker than average, but not the thickest ice measured. Its freeboard thickness (0.15 m) was close to average observed freeboard (0.14 ± 0.07 m). The contrast between ponded ice thickness and bare ice thickness was, however, the largest observed at all stations. Furthermore, this figure shows generally higher ratios for the 2011 observations, compared with 2010, on average. This reinforces the idea that the melt in 2011 had progressed further and that the ponds showed the effects of that melt more severely.

The enhanced transmittance by ponds is significant because of the large pond areal coverage for first-year ice. While the ice thickness may differ substantially for these two ice types, the most pronounced optical differences are almost entirely due to the presence of an SSL and a DL on bare, melting ice, and their conspicuous absence on ponded ice. As long as bare sea ice has positive freeboard and is melting, the formation of an SSL and a DL appear to be ubiquitous. Given their importance in determining the optical properties of the ice cover, we now explore the role of these thin, but optically important components of melting sea ice.

5.2. Relative Roles of Scattering Layers

Figure 11 shows model simulations illustrating the relative contributions of various scattering layers to the spectral albedo and transmittance. The (solid) black curves show the spectral albedo and transmittance from the 4DOM model developed for the 19 July 2011 study site. Removal of the top most centimeter, essentially the upper portion of the SSL (blue dot curve) and subsequent removal of the remainder of the SSL (top 3 cm; green dash-dot curve) promote significant decreases in albedo and increases in transmittance. In fact, this highly scattering layer is so important that removing a full meter of interior ice from the original model (red dash curve) is barely detectable in albedo, although it increases transmittance between 0.02 and 0.09 (18% on average). Finally, two curves show the albedo and transmittance for the case of only the bare interior ice found at ICESCAPE alone (cyan, dash-dot-dot) and the case of the first-year cold spring ice retrieved from Barrow (orange, short dash). The Barrow case is modeled without any snow, but of course, in situ, that ice was still snow covered. The SSL, and possibly the DL as well, appear to be essential to the preservation of a summer ice cover. Absence of these layers would result in significantly reduced albedo, such that the deficient ice cover would be expected to melt completely during a single summer. Thin or flooded ice may not have substantial freeboard to support a DL or even a thin SSL.

Furthermore, the model was used to test the effect of direct versus diffuse incident light conditions on measured transmittance. Differences were largest for ponded ice, in the absence of a surface scattering

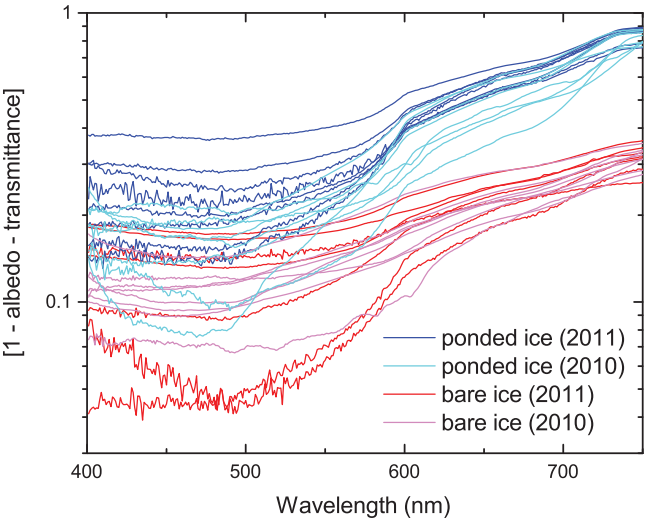

Figure 12. Spectral absorptivity calculated from observed spectral albedo and transmittance (1-albedo-transmittance).

layer. At wavelengths of peak transmittance (nominally 475–500 nm), the transmittance decreased by about 3% when the incident light was changed from diffuse (complete overcast, solar disk not visible) to direct (sunny, cloud free conditions). This change is subject to the low solar elevation angles typical of the Arctic. The highest transmittances that would be measured would occur under diffuse incident light conditions where at least a portion of the incident light is downward directed and transits the least possible optical depth of the ice. Bare ice cases showed negligible differences due to the high optical depths of the SSL and DL.

5.3. Spectral Absorptivity

Figure 12 shows estimates of spectral absorptivity (1-α-T) for all bare and ponded ice cases observed in this study. This total absorptivity is an indication of the amount of heat deposited within the ice. Average absorption by ponded ice exceeds absorption by bare ice at all wavelengths, but at wavelengths longer than 550 nm, the absorption by ponds is much greater. The difference is light that gets absorbed directly in the pond water and upper portions of the ice with little chance to backscatter to the atmosphere. This heat can melt ice, suggesting this absorption may be the primary mechanism for pond evolution (e.g., deepening and widening) during the melt season. The absorptivity of the bare ice was found to be approximately the same for 2010 and 2011. The absorptivity of the ponded ice, however, is generally higher in 2011, where pond albedos were typically lower and pond transmittances were typically higher. Once again reinforcing the idea that the ponds in 2011 showed the effects of melt more severely.

5.4. Comparison With Multiyear Ice

The average spectral albedos of bare and ponded first-year and multiyear ice are compared in Figure 13. While the albedo for bare first-year ice appears slightly smaller at all wavelengths than its multiyear counterpart, the standard deviations of the observations are large and the distinction is not significant. However, the physical characteristics of bare, melting first-year ice would be expected to yield a lower albedo than bare, melting multiyear ice. Physically, the most prominent difference between the two ice types is typically total ice thickness. The thinner first-year ice would necessarily have less freeboard and hence a thinner DL. A less substantial DL will result in reduced albedo. It is not clear whether this difference is seen in these observations, but, in an era of decreasing ice thickness, this study suggests that future reductions in albedo should be expected with diminishing DL thickness. Differences in the characteristic spectral shape may, or may not, be significant, or represent physical differences in the ice. Optical measurements made during the SHEBA campaign relied on legacy

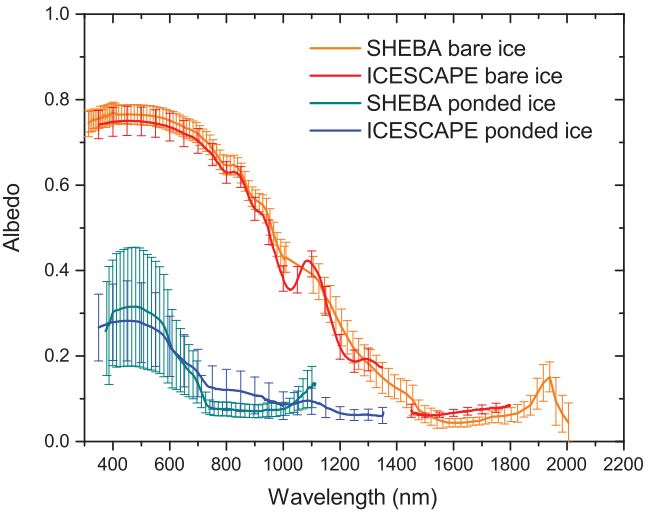

Figure 13. Average spectral albedos compared for bare and ponded ice as observed for multiyear ice during the SHEBA campaign [*Perovich et al.*, 2002] and first-year ice during ICESCAPE. ±1 standard deviation indicated.

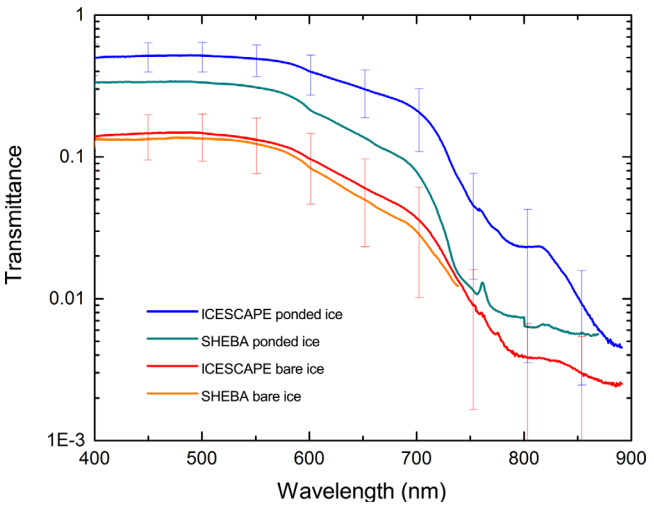

Figure 14. Average observed spectral transmittance of bare melting multiyear (SHEBA) compared with average first-year (ICESCAPE) bare and ponded ice.

instrumentation and it is possible that spectral differences (like the one centered at wavelength 1100 nm) may be entirely due to hardware limitations in the older instrumentation.

Average spectral albedos for ponded first-year and multiyear ice are also not significantly different, but the spectral albedos of ponds on multiyear ice clearly show larger variability. Multiyear ice has larger topography and a more variable ice history, and some of this variability translates to the appearance of the ponds. Ponds on multiyear ice span a range of conditions, from the flanks of ridges where the ponds appear bright blue, to darker blue sea level ponds on undeformed ice [*Perovich et al.*, 2002]. Much of the ICESCAPE variability is derived from differences between the 2010 melt ponds and the 2011 melt ponds, but during any one year, the ponds on first-year ice in a given region typically had relatively uniform appearance.

While differences between spectral albedo of first-year and multiyear bare and ponded ice types may be subtle, the differences in spectral transmittance are much more pronounced. Figure 14 shows average spectral transmittance for bare and ponded ice at SHEBA and ICESCAPE. While the bare ice transmittance is slightly larger for first-year ice, the more notable distinction is for ponded ice. On average, 50% more light is transmitted through the first-year ponded ice relative to multiyear ponded ice. The SHEBA ponds used to calculate the average transmittance in Figure 14 had average ice thickness 1.65 m, compared to the average pond floor thickness observed at ICESCAPE of 1.0 m. The ice beneath ponds on the multiyear ice may also have been optically thicker, possibly containing more bubbles, but that was not specifically characterized.

The inferred scattering coefficients presented in Table 1 also suggest reduced scattering in the ice interior compared to the parameterization put forth by *Briegleb and Light* [2007]. The inferred IOPs in that analysis were derived mostly from observations of multiyear ice during SHEBA. In particular, their guidance is for an interior scattering coefficient for bare ice of 20 m^{-1}, whereas, this analysis suggests an interior scattering coefficient reduced by 20%. This is more than the one standard deviation change in transmittance (15% change in scattering coefficient) identified by *Briegleb and Light* [2007]. Furthermore, the scattering coefficient recommended for ponded ice in their treatment was 20 m^{-1}, whereas the 13.4 m^{-1} found in the present analysis is close to the suggested one-standard deviation reduction. These results suggest that the parameterization of *Briegleb and Light* [2007] may underestimate light transmittance through a melting, ponded first-year sea ice cover.

5.5. Partitioning of Solar Radiation Within an Ice Cover

Light transmittance to the ocean is clearly larger for ponded ice than bare ice, but it is informative to consider what fraction of the incident light is absorbed within the ice itself. Heat deposited in the ice can further melt the ice locally, heat deposited into the ocean may become available to a different "class" of ice as ice advects, possibly promoting the complete melt of classes of very thin ice. It is also possible that light penetrating through the ice cover contributes significantly to heat storage in the so-called near surface temperature maximum [*Jackson et al.*, 2010]. Figure 15 shows the computed relative distribution of total solar heat (expressed as the percentage of incoming irradiance) backscattered, absorbed, and transmitted by ice representative of bare and ponded surface types observed during ICESCAPE and multiyear ice observed during SHEBA. The incident spectrum used for this calculation was measured during the ICESCAPE campaign and the same spectrum was applied to both cases.

For the bare ice cases, the thicker DL of multiyear ice absorbs twice as much heat as the thinner DL typical of first-year ice. The most notable difference, however, is between the absorption by interior ice in the bare

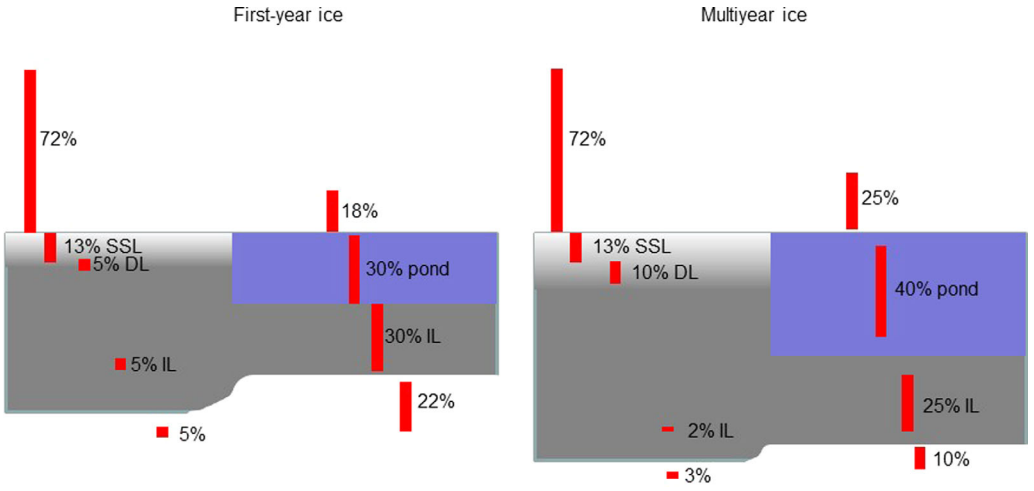

Figure 15. Relative distribution of total solar heat backscattered, absorbed and transmitted in bare and ponded first-year ice compared for representative first-year sea ice and multiyear sea ice.

and ponded cases. With no SSL or DL to backscatter light at the surface of ponded ice, more light propagates deeper into the ice cover where it is absorbed. This is illustrated by comparing the 25–30% of incident light absorbed in the IL beneath ponds compared with the 2–5% absorbed beneath the SSL and DL of bare ice. The SSL and DL act as "armor" for the bare ice, and the SSL appears to be readily renewed by the absorption of solar radiation, as noted by *Perovich et al.* [2002]. The significantly increased absorption within ponded ice contributes to local melting and thinner ice. In fact, ponds lose their ability to backscatter light as they deepen and pond floors thin, and this additional heat absorbed in pond water and pond floors may also contribute to the evolution of the optical properties of ponded ice.

We have little quantitative knowledge of the seasonal progression of sea ice optical properties. *Light et al.* [2008] showed some evolution of IOPs during the course of the summer for the multiyear ice observed at SHEBA, where the SSL and DL have the most obvious progressions. The interior of multiyear ice showed little variation during the course of the summer melt season. The seasonal evolution of FY ice optical properties has not yet been documented. Data collected on the cold spring first-year ice at Barrow (see Figure 8) suggest that during the early season, scattering in the ice interior is small, as individual brine and gas inclusions are small and isolated. This ice was still snow covered, so the albedo of such bare ice is mostly irrelevant, and the onset of its melt will be marked by the development of an SSL and a DL. However, there are also changes as the interior ice evolves from low scattering in spring to higher scattering in summer. The evolution of optical properties as sea ice transitions from first-year ice to multiyear ice also needs to be investigated.

6. Conclusions

Measurements made at 19 study sites over two summers indicate that ponded first-year ice transmits 1.3 to nearly 10 times more light at wavelengths of peak transmittance than adjacent bare ice. This corresponds to the transmission of roughly 4.4 times more total energy into the ocean (Figure 15). Estimates of typical bare, first-year ice transmitted fluxes range from 13 to 56 W m^{-2} (where incident flux is estimated to be 541 W m^{-2}). Transmitted fluxes under adjacent ponded ice are typically 75–130 W m^{-2}. These estimates correspond with peak planar PAR irradiance values of 143.2 μmol s^{-1} m^{-2} (bare) and 752.9 μmol s^{-1} m^{-2} (ponded), both measured at Station 101 in 2011. These values are significant because of the documented increases in pond areal fraction for first-year ice [*Fetterer and Untersteiner*, 1998; *Eicken et al.*, 2004; *Perovich et al.*, 2011; *Perovich and Polashenski*, 2012].

The ubiquitous surface-scattering and drained layers present on bare ice are almost entirely responsible for the relatively high albedo of bare, melting ice. These layers appear to form rapidly as the snow melts [*Perovich et al.*, 2003]. Without these layers, bare ice albedo at 500 nm would be roughly 0.1–0.5 less than observed, a decrease that could likely promote the complete and rapid melt of the ice cover. We speculate that mechanisms for the removal or reduction of this surface layer may include decreased freeboard height due to

decreased ice thickness or the inundation of these layers due to surface flooding. Interestingly, changes in ice thickness (as long as the ice thickness remains larger than about 0.5 m) have little direct effect on observed bare ice albedo, but changes in ice thickness have large impact on the thickness and scattering coefficient of the drained layer and possibly even the surface scattering layer. The DL is thus an essential element of an optical property model for sea ice, since it is a critical link between the thickness of the ice and the vertical variation of its optical properties. With no SSL or DL on ponded ice, the optical properties of that ice type are determined exclusively by the depth of the pond and the properties of the interior ice beneath the standing water.

The most notable difference between the optical properties of first-year and multiyear ice appears to be the distinction between light transmittance through the two ice types. Transmittance through bare ice appears to depend largely on the properties of the SSL and DL, and these properties appear somewhat invariant across ice types. Light transmission through ponded ice, however, depends much more strongly on the physical thickness of the ice and the magnitude of the scattering coefficient in the interior ice.

All of these factors describe an ice cover whose light partitioning is largely determined by the fractional coverage of melt ponds. While bare ice has characteristically high albedo, and relatively small heat absorption within the ice and transmittance to the ocean, ponded ice has characteristically low albedo and significant heat absorption within the ice and transmittance to the ocean. Bare ice reflects nearly three-quarters of the incident sunlight and is somewhat resilient to melting by shortwave insolation. In contrast, ponded ice absorbs or transmits three-quarters of the incident sunlight and its thickness is much more vulnerable to melting by the absorption of shortwave radiation.

Investigation of the seasonal evolution of the IOPs of sea ice is needed. Results from this study indicate that cold, springtime first-year sea ice has very small scattering, and this scattering increases by the time the ice cover has fully developed melt ponds. The pathways by which the interior scattering increases, the onset and development of a surface scattering layer and drained layer, and the fate of ice that lasts through the melt season has not been investigated. Time-dependent observations of the optical properties of first-year sea ice through the inception and full development of melt, and in particular the evolution of the properties of the surface scattering and drained layers, would be a strong addition to our knowledge of how sunlight is partitioned by a seasonal ice cover.

Acknowledgments

The data for this paper are archived at NASA's Ocean Biology Processing Group repository (SeaBASS) http://seabass.gsfc.nasa.gov/seabasscgi/archive.cgi?q=CRREL/perovich/icescape. We thank K. Colburn for her capable assistance handling the data. This research was supported by the NASA Impacts of Climate change on the Ecosystems and Chemistry of the Arctic Pacific Environment (ICESCAPE) project with support from the NASA Cryospheric Sciences Program (grant NNH10A017I to D. Perovich and B. Light) and the NASA Ocean Biology and Biogeochemistry Program. Subcontract to the University of Washington from NASA parent grant NNX14AH61G to K. Frey, Clark University is gratefully acknowledged. This work would not have been possible without the capable and professional support of the USCGC Healy crew during two field seasons of the ICESCAPE project. Comments from S. Hudson and one anonymous reviewer helped to improve this paper.

References

Briegleb, B. P., and B. Light (2007), A delta-Eddington multiple scattering parameterization for solar radiation in the sea ice component of the Community Climate System Model, *NCAR Tech. Note TN-4721STR*, 100 pp., Nat. Cent. Atmos. Res., Boulder, Colo.

Comiso, J. C. (2012), Large decadal decline of the Arctic multiyear ice cover, *J. Clim.*, *25*(4), 1176–1193, doi:10.1175/JCLI-D-11-00113.1.

Ebert, E. E., J. L. Schramm, and J. A. Curry (1995), Disposition of solar radiation in sea ice and the upper ocean, *J. Geophys. Res.*, *100*(C8), 15,965–15,975, doi:10.1029/95JC01672.

Ehn, J. K., T. N. Papakyriakou, and D. G. Barber (2008), Inference of optical properties from radiation profiles within melting landfast sea ice, *J. Geophys. Res.*, *113*, C09024, doi:10.1029/2007JC004656.

Eicken, H., T. C. Grenfell, D. K. Perovich, J. A. Richter-Menge, and K. Frey (2004), Hydraulic controls of summer Arctic pack ice albedo, *J. Geophys. Res.*, *109*, C08007, doi:10.1029/2003JC001989.

Fernández-Méndez, M., C. Katlein, B. Rabe, M. Nicolaus, I. Peeken, K. Bakker, H. Flores, and A. Boetius (2015), Photosynthetic production in the central Arctic Ocean during the record sea-ice minimum in 2012, *Biogeosciences*, *12*(11), 3525–3549, doi:10.5194/bg-12-3525-2015.

Fetterer, F., and N. Untersteiner (1998), Observations of melt ponds on Arctic sea ice, *J. Geophys. Res.*, *103*(C11), 24,821–24,835, doi:10.1029/98JC02034.

Frey, K. E., D. K. Perovich, and B. Light (2011), The spatial distribution of solar radiation under a melting Arctic sea ice cover, *Geophys. Res. Lett.*, *38*, L22501, doi:10.1029/2011GL049421.

Grenfell, T. C. (1991), A radiative transfer model for sea ice with vertical structure variations, *J. Geophys. Res.*, *96*(C9), 16,991–17,001, doi:10.1029/91JC01595.

Grenfell, T. C., and G. A. Maykut (1977), The optical properties of ice and snow in the Arctic Basin, *J. Glaciol.*, *18*(80), 445–463.

Grenfell, T. C., and D. K. Perovich (2004), Seasonal and spatial evolution of albedo in a snow-ice-land-ocean environment, *J. Geophys. Res.*, *109*, C01001, doi:10.1029/2003JC001866.

Hamre, B., J. Winther, S. Gerland, J. J. Stamnes, and K. Stamnes (2004), Modeled and measured optical transmittance of snow-covered first-year sea ice in Kongsfjorden, Svalbard, *J. Geophys. Res.*, *109*, C10006, doi:10.1029/2003JC001926.

Holland, M. M., D. A. Bailey, B. P. Briegleb, B. Light, and E. Hunke (2012), Improved sea ice shortwave radiation physics in CCSM4: The impact of melt ponds and aerosols on Arctic sea ice, *J. Clim.*, *25*(5), 1413–1430, doi:10.1175/JCLI-D-11-00078.1.

Hudson, S. R., M. A. Granskog, A. Sundfjord, A. Randelhoff, A. H. H. Renner, and D. V. Divine (2013), Energy budget of first-year Arctic sea ice in advanced stages of melt, *Geophys. Res. Lett.*, *40*, 2679–2683, doi:10.1002/grl.50517.

Inoue, J., T. Kikuchi, and D. K. Perovich (2008), Effect of heat transmission through melt ponds and ice on melting during summer in the Arctic Ocean, *J. Geophys. Res.*, *113*, C05020, doi:10.1029/2007JC004182.

Jackson, J. M., E. C. Carmack, F. A. McLaughlin, S. E. Allen, and R. G. Ingram (2010), Identification, characterization, and change of the near-surface temperature maximum in the Canada Basin, 1993–2008, *J. Geophys. Res.*, *115*, C05021, doi:10.1029/2009JC005265.

Jin, Z., K. Stamnes, W. F. Weeks, and S. Tsay (1994), The effect of sea ice on the solar energy budget in the atmosphere-sea ice-ocean system: A model study, *J. Geophys. Res.*, *99*(C12), 25,281–25,294, doi:10.1029/94JC02426.

Kwok, R., G. F. Cunningham, M. Wensnahan, I. Rigor, H. J. Zwally, and D. Yi (2009), Thinning and volume loss of the Arctic Ocean sea ice cover: 2003–2008, *J. Geophys. Res.*, *114*, C07005, doi:10.1029/2009JC005312.

Light, B., G. A. Maykut, and T. C. Grenfell (2003), A two-dimensional Monte Carlo model of radiative transfer in sea ice, *J. Geophys. Res.*, *108*(C7), 3219, doi:10.1029/2002JC001513.

Light, B., T. C. Grenfell, and D. K. Perovich (2008), Transmission and absorption of solar radiation by Arctic sea ice during the melt season, *J. Geophys. Res.*, *113*, C03023, doi:10.1029/2006JC003977.

Logvinova, C. L., K. E. Frey and L. W. Cooper (in review), The role of sea ice melt in the distribution of chromophoric dissolved organic matter in the Chukchi and Beaufort seas. Deep-Sea Research Part II: Topical Studies in Oceangraphy.

Manabe, S., and R. J. Stouffer (1980), Sensitivity of a global climate model to an increase of CO_2 concentration in the atmosphere, *J. Geophys. Res.*, *85*(C10), 5529–5554, doi:10.1029/JC085iC10p05529.

Maslanik, J. A., C. Fowler, J. Stroeve, S. Drobot, J. Zwally, D. Yi, and W. Emery (2007), A younger, thinner Arctic ice cover: Increased potential for rapid, extensive sea-ice loss, *Geophys. Res. Lett.*, *34*, L24501, doi:10.1029/2007GL032043.

Maykut, G. A., and M. G. McPhee (1995), Solar heating of the Arctic mixed layer, *J. Geophys. Res.*, *100*(C12), 24,691–24,703, doi:10.1029/95JC02554.

Nghiem, S. V., I. G. Rigor, D. K. Perovich, P. Clemente-Colon, J. W. Weatherly, and G. Neumann (2007), Rapid reduction of Arctic perennial sea ice, *Geophys. Res. Lett.*, *34*, L19504, doi:10.1029/2007GL031138.

Nicolaus, M., S. Gerland, S. R. Hudson, S. Hanson, J. Haapala, and D. K. Perovich (2010), Seasonality of spectral albedo and transmittance as observed in the Arctic Transpolar Drift in 2007, *J. Geophys. Res.*, *115*, C11011, doi:10.1029/2009JC006074.

Nicolaus, M., C. Katlein, J. Maslanik, and S. Hendricks (2012), Changes in Arctic sea ice result in increasing light transmittance and absorption, *Geophys. Res. Lett.*, *39*, L24501, doi:10.1029/2012GL053738.

Nicolaus, M., C. Petrich, S. R. Hudson, and M. A. Granskog (2013), Variability of light transmission through Arctic land-fast sea ice during spring, *Cryosphere*, *7*(3), 977–986, doi:10.5194/tc-7-977-2013.

Palmer, M., G. van Dijken, B. G. Mitchell, B. J. Seegers, K. E. Lowry, M. M. Mills, and K. R. Arrigo (2013), Light and nutrient control of photosynthesis in natural phytoplankton populations from the Chukchi and Beaufort seas, Arctic Ocean, *Limnol. Oceanogr.*, *58*(6), 2185–2205.

Perovich, D. K. (2005), On the aggregate-scale partitioning of solar radiation in Arctic sea ice during the Surface Heat Budget of the Arctic Ocean (SHEBA) field experiment, *J. Geophys. Res.*, *110*, C03002, doi:10.1029/2004JC002512.

Perovich, D. K., and C. Polashenski (2012), Albedo evolution of seasonal Arctic sea ice, *Geophys. Res. Lett.*, *39*, L08501, doi:10.1029/2012GL051432.

Perovich, D. K., et al. (1998), Field observations of the electromagnetic properties of first-year sea ice, *IEEE Trans. Geosci. and Rem. Sens.* *36*(5), 1705–1715.

Perovich, D. K., T. C. Grenfell, B. Light, and P. V. Hobbs (2002), Seasonal evolution of the albedo of multiyear Arctic sea ice, *J. Geophys. Res.*, *107*(C10), 8044, doi:10.1029/2000JC000438.

Perovich, D. K., T. C. Grenfell, J. A. Richter-Menge, B. Light, W. B. I. Tucker, and H. Eicken (2003), Thin and thinner: Sea ice mass balance measurements during SHEBA, *J. Geophys. Res.*, *108*(C3), 8050, doi:10.1029/2001JC001079.

Perovich, D. K., K. F. Jones, B. Light, H. Eicken, T. Markus, J. Stroeve, and R. Lindsay (2011), Solar partitioning in a changing Arctic sea-ice cover, *Ann. Glaciol.*, *52*(57), 192–196, doi:10.3189/172756411795931543.

Untersteiner, N. (1961), On the mass and heat budget of Arctic sea ice, *Arch. Meteorol. Geophys. Bioklimatol., Ser. A*, *12*, 151–182.